SPATIAL COHERENCE THEORY AND ITS APPLICATION TO SYNTHETIC APERTURE SYSTEMS

Daniel C. Brown, Applied Research Laboratory, Penn State University, USA
Anthony P. Lyons, Applied Research Laboratory, Penn State University, USA
Daniel A. Cook, Georgia Tech Research Institute, Atlanta, USA

1 INTRODUCTION

Synthetic aperture systems coherently integrate data collected over space and time to produce high resolution imagery. The signal processing strategies employed exploit both the temporal and spatial coherence of the field scattered by the scene. Standard stripmap or spotlight imagery is formed by coherent combination of multiple azimuthal looks at a scene over a wide range of observed aspects. In interferometric processing, spatial coherence between a pair of images collected on vertically displaced antennae is required to produce an estimate of the differential phase between the images. This differential phase may then be inverted to provide an estimate of the scene's topography or bathymetry. Interferometric synthetic aperture systems have shown there is an upper bound on the collection baseline for the majority of the pixels in the scene to maintain coherence; however, some points, called permanent scatterers, have a much larger temporal and spatial coherence length. Foliage Penetrating (FOPEN) systems exploit the temporal and spatial coherence of the scattered field to segment targets obscured by a foliage background.

The temporal coherence length of the scattered field is determined by the time scale of the disturbance of the scattering surface. Jackson *et al.*[1] investigated the temporal coherence of seafloor scattering. In this model, the roughness of the scene is continuously modified through biologic processes (e.g. fish and invertebrate feeding). This is modeled as a diffusion process and this model has been applied to repeat-pass, SAS, coherent change detection by Lyons and Brown[2] to explain the temporal coherence lengths observed for a rail-mounted SAS system. Radar systems utilize a similar model to define exponential decay times for the coherence for windblown clutter[3].

In order to focus this paper we restrict our attention to the spatial coherence of the scattered field. To support this analysis we will use the van Cittert-Zernike theorem (vCZT) which has been developed in the field of statistical optics to calculate the spatial coherence of the field radiated from an incoherent radiator. This theorem has been successfully applied to both acoustic[4,5] and radar[6] scattering problems. In Section 2 the van Cittert-Zernike theorem is reviewed and shown to provide a model for the spatial coherence of the field scattered from within a scene. This theory will be used to discuss the impact of spatial coherence on several areas including: interferometric baseline decorrelation (Section 3); aperture coherence and target enhancement (Section 4); and estimation of along-track motion error for Vernier SAS array (Section 5).

2 SPATIAL COHERENCE OF THE SCATTERED FIELD

The field scattered from a scene is composed of two components with different spatial coherence lengths. The specular, or coherent, component of the scattered field is that portion reflected from the scene in phase with the original transmit signal. That is, the scattering interaction does not perturb the phase of the transmitted waveform, and the returned signal is a copy of the transmitted waveform that is scaled due to reflection coefficient and propagation loss. The diffuse, or incoherent, component of the scattered field is that portion where the scattering interaction has randomized the phase of the original transmit signal. The coherent component of the scattered field is associated with scattering from smooth interfaces of finite size, corners or edges and is broadly spatially co-

The author gratefully acknowledges the US Office of Naval Research for its support of this work (Grant Number: N00014-14-1-0566).

herent. The incoherent component is associated with scattering from rough interfaces and is more narrowly spatially coherent. The difference in the coherence lengths associated with the coherent and incoherent fields has been observed for seafloor scattering by Clay[7].

The spatial coherence of the field scattered from a surface of arbitrary roughness may be calculated using the theory of partial coherence developed in statistical optics. A summary of the work in this area can be found in several texts[8–11]. A pair of signals received at positions Q_1 and Q_2 are given by

$$u(Q_1, t+\tau) = -\frac{jk}{2\pi} \iint_{\sigma} \frac{u(P_1, t+\tau-\frac{R_1}{c})}{R_1} \, \mathrm{d}S_1 \tag{1}$$

$$u(Q_2, t) = \frac{jk}{2\pi} \iint_{\sigma} \frac{u(P_2, t-\frac{R_2}{c})}{R_2} \, \mathrm{d}S_2, \tag{2}$$

where c is the speed of propagation, k is the wavenumber, and τ is the delay. The mutual coherence, or correlation, may be defined as

$$\Gamma(Q_1, Q_2, \tau) = \langle u(Q_1, t+\tau) u^*(Q_2, t) \rangle, \tag{3}$$

where the geometry is defined in Figure 1.

$$\Gamma(Q_1, Q_2, \tau) = \frac{k^2}{4\pi^2} \iint_{\sigma} \iint_{\sigma} \frac{\langle u(P_1, t+\tau-\frac{R_1}{c}) u^*(P_2, t-\frac{R_2}{c}) \rangle}{R_1 R_2} \, \mathrm{d}S_1 \, \mathrm{d}S_2 \tag{4}$$

$$\Gamma(Q_1, Q_2, \tau) = \frac{k^2}{4\pi^2} \iint_{\sigma} \iint_{\sigma} \frac{\Gamma(P_1, P_2, \tau+\frac{R_2-R_1}{c})}{R_1 R_2} \, \mathrm{d}S_1 \, \mathrm{d}S_2 \tag{5}$$

Evaluating the scattered field at zero lag gives the mutual intensity

$$J(Q_1, Q_2) = \Gamma(Q_1, Q_2, \tau = 0). \tag{6}$$

Under a narrowband approximation, the mutual coherence on the surface σ can be expressed in terms of the mutual intensity as

$$\Gamma(P_1, P_2, \frac{R_2 - R_1}{c}) = J(P_1, P_2) \exp\left[-jk(R_2 - R_1)\right]. \tag{7}$$

Making this substitution gives

$$J(Q_1, Q_2) = \frac{k^2}{4\pi^2} \iint_{\sigma} \iint_{\sigma} \frac{J(P_1, P_2)}{R_1 R_2} \exp\left[-jk(R_2 - R_1)\right] \, \mathrm{d}S_1 \, \mathrm{d}S_2. \tag{8}$$

In the case of a surface with sufficient roughness, the scattered field is incoherent and the mutual intensity is given by

$$J(P_1, P_2) \propto I(P_1) \delta(|P_1 - P_2|) \tag{9}$$

The sifting property of the delta function reduces Equation 8 to a single integral over the surface σ, Figure 2. This yields the following expression for the mutual intensity

$$J(Q_1, Q_2) \propto \frac{k^2}{4\pi^2} \iint_{\sigma} \frac{I(P_1)}{R_1 R_2} \exp\left[-jk(R_2 - R_1)\right] \, \mathrm{d}S_1. \tag{10}$$

This is the van Cittert-Zernike theorem, and it states that the spatial coherence of the incoherent component of the scattered field is determined by the spatial distribution of the scattering intensity over the scene.

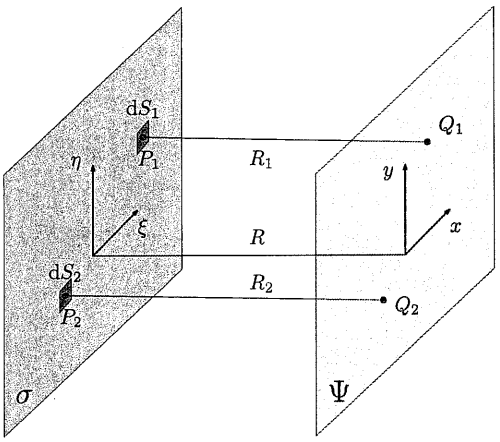

Figure 1: Geometry for calculation of the mutual intensity of an arbitrary coherence radiator

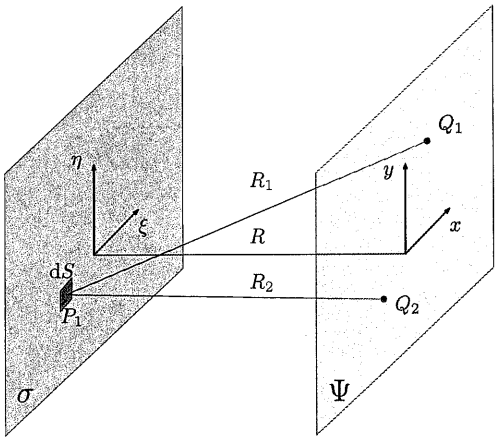

Figure 2: Geometry for calculation of the mutual intensity of an incoherent radiator

3 INTERFEROMETRIC BASELINE DECORRELATION

Interferometric processing of synthetic aperture radar[6] and sonar[12] data is used to extract information from the phase of the imagery collected over a scene. While the basis for interferometric processing is the same for radar and sonar, there are several important differences in the collection geometry that impact the spatial coherence across the interferometer.

In this section, we restrict ourselves to discussing cross-track interferometers, where the goal is the estimation of the topography or bathymetry of the imaged scene from the differential phase between a pair of synthetic aperture collections with vertically offset antennae. The differential phase stability is determined in part by the coherence between the two component images. The spatial coherence of the incoherent component of the scattered field limits the maximum spatial separation, or baseline, between the receivers on the synthetic aperture system. This "baseline decorrelation" was described by Zebker and Villasensor[13] as one of several noise sources that may degrade the coherence in an interferometric system.

Zebker and Villasensor model the spatial coherence of the scattered field using the van Cittert-Zernike theorem as defined in Equation 10. Normalizing this equation by the autocorrelation gives an estimate of the correlation coefficient

$$\rho_{\text{baseline}} = \frac{J(Q_1, Q_2)}{\sqrt{J(Q_1, Q_1) J(Q_2, Q_2)}}. \tag{11}$$

Assuming the impulse response of the system is modeled as a sinc function in range and evaluating Equation 10 we find

$$\rho_{\text{baseline}} = 1 - \frac{2|\delta\theta|\delta_x \cos\theta}{\lambda}, \tag{12}$$

where the collection geometry is shown in Figure. 3. Setting $\rho_{\text{baseline}} = 0$ and defining the component of the baseline perpendicular to the look direction as

$$B_\perp = R\delta\theta, \tag{13}$$

we can solve for the critical baseline where the correlation coefficient between the two looks is zero

$$B_{\perp,\,\text{crit}} = \frac{\lambda R}{2\delta_x \cos\theta}. \tag{14}$$

In Figure 4, $B_{\perp,\,\text{crit}}$ is compared for an InSAS (HISAS-1030) and a pair of space-borne InSAR systems (COSMO-SkyMed and TanDEM-X). The modeled parameters for these systems are given in

Table 1. The critical baseline is calculated for each system across the range of operating incidence angles.

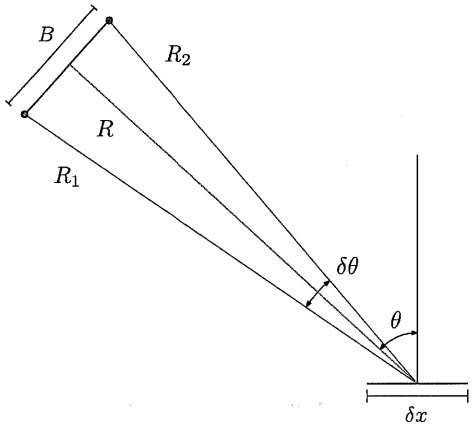

Figure 3: Interferometric Collection Geometry

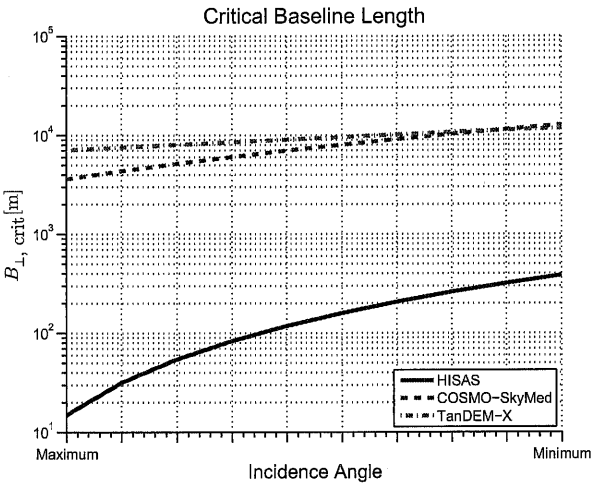

Figure 4: InSAR and InSAS critical baselines are determined by their imaging geometries

Parameter	HISAS[12]	COSMO-SkyMed[14]	TanDEM-X[15]
Frequency (f_0)	100 kHz	9.6 GHz	9.6 GHz
Wavelength (λ)	1.5 cm	3.1 cm	3.1 cm
Range Resolution (δ_x)	0.02 m	3 m	1.5 m
Altitude	20 m	619 km	515 km
Incidence Angle (θ)	45-82 deg	20-60 deg	30-48 deg

Table 1: Interferometric SAS and SAR System Operating Parameters

Permanent scatterer InSAR utilizes the stability of the phase of the pixels within a scene that are dominated by the coherent scattering component. These pixels are called permanent scatterers and they support larger baselines without decorrelation. Permanent scatterers are formed when a pixel has a single dominant scatter within it. For example, in an urban area the permanent scatterers may be due to sub-pixel metal objects (e.g. railings, street lights). This form of InSAR was first proposed by Ferretti, Prati and Rocca[16], and it has been found to be successful over urban areas where the density of permanent scatterers is sufficient to map the height field.

4 APERTURE COHERENCE AND TARGET ENHANCEMENT

The field scattered from targets within a scene is composed of a coherent and an incoherent component. In Section 3, the presence of permanent scatterers was attributed to dominant targets whose extent is smaller than a resolution cell, where the field scattered from the target is coherent over the full aperture. Manmade targets that are larger than a resolution cell may produce fields that are coherent over only a portion of the supported aperture. This aspect-dependence of the scattering strength has been exploited by Chaney, Willsky, and Novak to develop an adaptive beamformer to increase the detectability of manmade targets in foliage penetrating (FOPEN) SAR systems[17].

A related approach for improving the target-to-background ratio for a proud cylinder is shown in Figure 5. A scene with a cylindrical target (length 60 cm and diameter 30 cm) has been simulated using PC-SWAT[18]. The simulated sonar operates over the band 15-25 kHz with a total beamwidth in excess of 60 degrees. A segment of the image centered on the target is shown in Figure 5(a). In this simulation, the raw data was contaminated with additive noise to produce an image with a poor target-to-background ratio. The complex target strength[19,20], which is a frequency/azimuth representation of the scattered field, is calculated for an image segment containing the cylindrical target, Figure 5(b). The correlation coefficient between all pairs of target-strength aspects is then calculated and shown in Figure 5(c). Near the specular direction (8.5 degrees), the coherence length is larger due to the spatial coherence of the coherent component of the scattered field. Using this figure, the scattered field is estimated to be coherent over the range of aspects from 6-11 degrees. The original image is processed using a k-space filter to extract only these aspects and the output of this process is shown in Figure 5(d). The original dimension of the target has been maintained, while the target-to-background ratio has been improved by restricting the image to those aspects that contain the specular response.

5 SAS ALONG-TRACK MOTION ESTIMATION

Another problem of interest in the field of SAS is that of estimating errors in the along-track direction. The displaced phase center (DPC) motion estimation technique relies on the correlation between overlapping channels between two consecutive pings to estimate the platform motion. This implies that the SAS system is capable of measuring its speed with sufficient accuracy to ensure that the DPC channels overlap properly. This is typically accomplished by slaving the SAS ping timing to an externally referenced speed over ground sensor. The distance covered between pings is known as the advance per ping or APP. Errors in APP have two deleterious effects on the SAS operation. First, the array may become spatially aperiodically sampled. As long as the APP error is not severe, this poses little difficulty if the true APP is known. The other effect of APP errors is to reduce the correlation of the DPC pairs.

Groen[21], Oeschger[22], and Cook[23] each describe techniques for the estimation of the APP error from SAS data. In each case, the correlation coefficient is measured between sets of phase centers spanning the expected range of advances. These measured correlations are then interpolated to find the ideal advance length. While Groen and Cook do not suggest an interpolation kernel, Oescheger recommends using a quadratic interpolator. Mallart and Fink[4] use the van Cittert-Zernike theorem to study the spatial coherence of the scattered field in ultrasound. In their analysis the intensity, $I(P_1, P_2)$, in Equation 10 is given by the projection of the transmit beampattern $b(\theta) = \mathrm{sinc}^2(\frac{D}{\lambda}\sin\theta)$ onto the scene. This results in a spatial coherence that is well modeled by a triangle function. This suggests that a triangle function may be an appropriate interpolation kernel. For systems where both the receiver and transmitter are directive we have simulated the spatial coherence using Equation 10 and found the resulting spatial coherence is well modeled as a Gaussian. In Figure 6 we compare the along-track spatial coherence for a 120 kHz SAS operating with a 5 cm wide transmitter and receive array that has a channel width and center-to-center spacing of 5 cm. The simulated coherence is shown compared to the best fit quadratic, triangle and Gaussian functions. A Monte-Carlo simulation is then run, where the APP is simulated with errors ranging over ± 1.25 cm. The APP is estimated for each iteration of the simulation using the interpolation kernels in Figure 6. The resulting APP bias errors are shown as a function of APP error in Figure 7. Here we see that the Gaussian form, which best matches the van Cittert-Zernike theorem modeled coherence, produces a result with reduced bias errors when compared to the other interpolation kernels.

6 CONCLUSION

We have discussed the importance of spatial coherence for three synthetic aperture applications: interferometric baseline decorrelation, adaptive target enhancement, and SAS along-track motion estimation. In each, it was shown that the coherent nature of the field scattered by the scene may

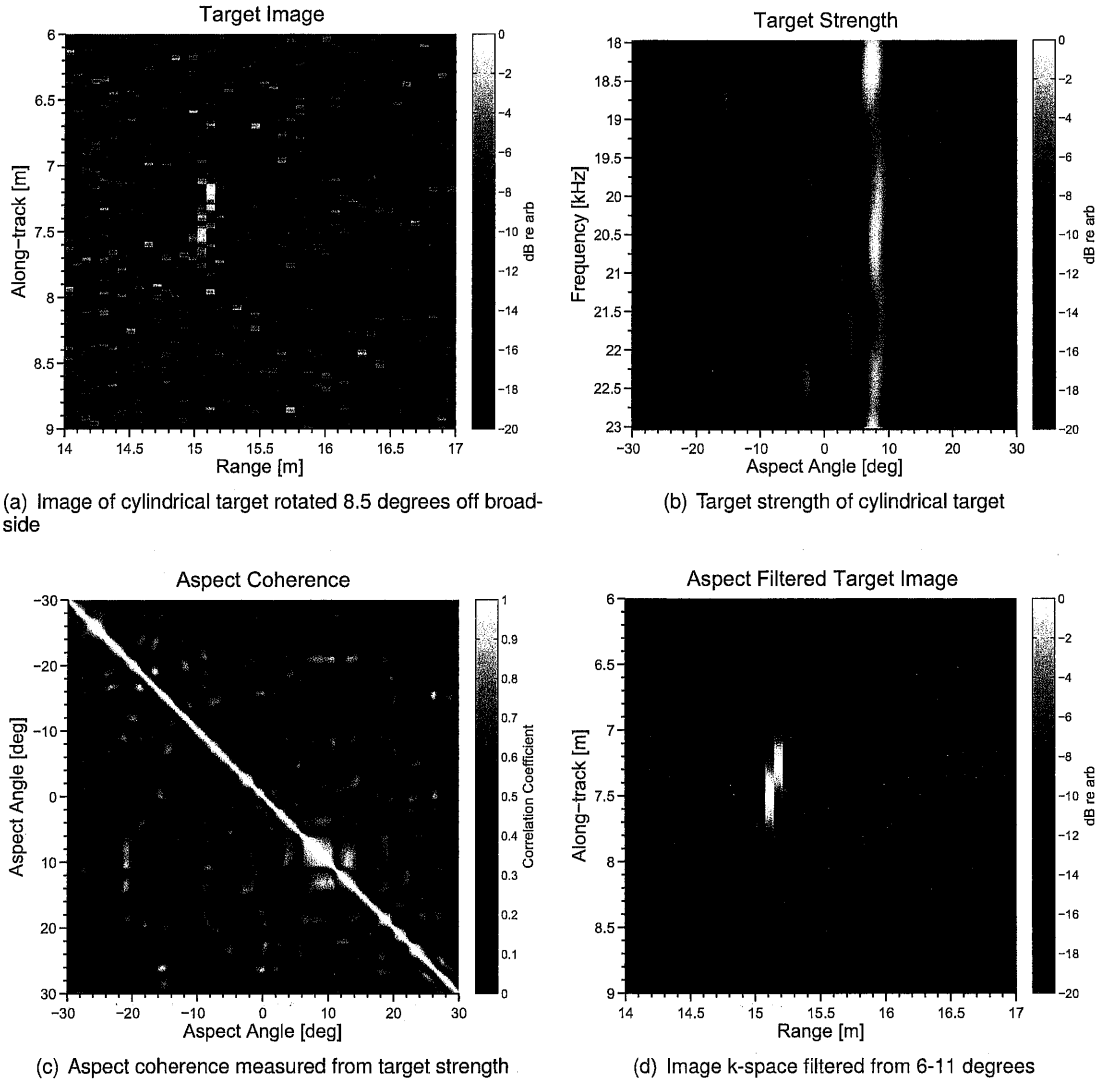

(a) Image of cylindrical target rotated 8.5 degrees off broadside

(b) Target strength of cylindrical target

(c) Aspect coherence measured from target strength

(d) Image k-space filtered from 6-11 degrees

Figure 5: The SNR on the 60 cm length cylinder is improved by adaptively modifying the integration aperture based on the spatial coherence of the scattered field

impact the performance of the system. We have reviewed a derivation of the van Cittert-Zernike theorem and shown its utility as a tool for estimation of the spatial coherence of the incoherent component of the field. This theorem was applied to study the collection geometry of InSAR and InSAS systems. The limited spatial coherence of the incoherent field, which dominates the majority of the pixels in a scene, limits the usable antenna baseline length. To avoid this limitation permanent scatterer interferometric systems identify the subset of pixels in the scene dominated by the coherent field. The larger spatial coherence length of the coherent field allows these points to be processed with larger baselines, which results in higher topographic accuracy.

The longer coherence length of the coherent field was utilized in a technique for the enhancement of manmade targets. A SAS image of a cylindrical target in an elevated noise environments was simulated. This target produced a scattered field with a significant coherent component over a limited portion of the synthetic aperture. Using aspect-to-aspect correlation, it is possible to measure the portion of the synthetic aperture where the targets scattered field is coherent. Subsequent k-space filtering, to select the coherent portion of the synthetic aperture, improved the target-to-background

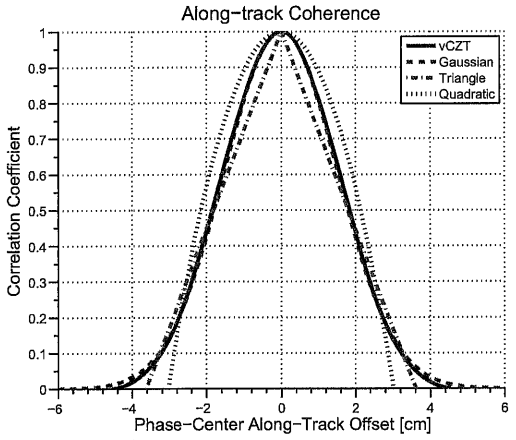

Figure 6: The along-track spatial coherence for a system with directional transmit and receive beams is best modeled using a Gaussian function

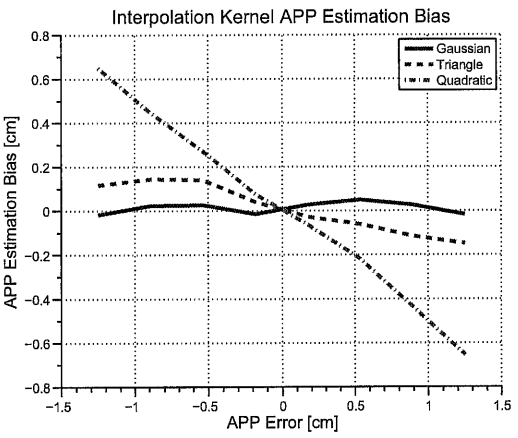

Figure 7: APP estimation bias errors are minimized by matching the interpolation kernel to the spatial coherence

ratio. Future work will be directed toward automating this process of identifying the coherent portion of the aperture and designing the corresponding k-space filter.

Finally, we have addressed the problem of SAS along-track motion estimation. In dynamic environments, where the spatial sampling of the aperture may be irregular, it is necessary to estimate the along-track component of the instrument's trajectory. This requires interpolation of the measured DPC correlation coefficients to determine the APP error. We have shown that the functional form of the interpolation kernel must be matched to the spatial coherence of the field to avoid estimation bias errors.

References

1. D. R. Jackson, M. D. Richardson, K. L. Williams, A. P. Lyons, C. D. Jones, K. B. Briggs, and D. Tang, "Acoustic observation of the time dependence of the roughness of sandy seafloors," *IEEE J. Oceanic Eng.*, vol. 34, no. 4, pp. 407–422, Oct. 2009.

2. A. P. Lyons and D. C. Brown, "Temporal variability of seafloor roughness and its impact on coherent change detection," in *Proc. Institute of Acoustics*, vol. 32, no. 4, Lerici, Italy, 2010, pp. 7–12.

3. J. B. Billingsley, "Exponential decay in windblown radar ground clutter doppler spectra: Multifrequency measurements and model," Lincoln Laboratory, Lexington, MA, Tech. Rep. ESC-TR-95-098, July 1996.

4. R. Mallart and M. Fink, "The van Cittert-Zernike theorem in pulse echo measurements," *J. Acoust. Soc. Am.*, vol. 90, no. 5, pp. 2718–2727, 1991.

5. P. H. Dahl, "Forward scattering from the sea surface and the van Cittert-Zernike theorem," *J. Acoust. Soc. Am.*, vol. 115, no. 2, pp. 589–599, 2004.

6. P. A. Rosen, S. Hensley, I. R. Joughin, F. K. LI, S. N. Madsen, E. Rodríguez, and R. M. Goldstein, "Synthetic aperture radar interferometry," *Proc IEEE*, vol. 88, no. 3, pp. 333–382, Mar. 2000.

7. C. S. Clay, "Coherent reflection of sound from the ocean bottom," *J. Geophys. Res.*, vol. 71, no. 8, pp. 2037–2046, 1966.

8. M. J. Beran and G. B. Parrent, *Theory of Partial Coherence*. Prentice-Hall, 1964.

9. J. W. Goodman, *Statistical Optics*. New York, NY: John Wiley and Sons, 1985.

10. J. Peřina, *Coherence of Light*. D. Reiddel Publishing, 1985.

11. M. Born and E. Wolf, *Principles of Optics*, 7th ed. New York: Cambridge University Press, 1999.

12. T. O. Sæbø, "Seafloor depth estimation by means of interferometric synthetic aperture sonar," Ph.D. dissertation, University of Tromsø, Sep. 2010.

13. H. A. Zebker and J. Villasenor, "Decorrelation in interferometric radar echos," *IEEE Trans. Geosci. Remote Sensing*, vol. 30, no. 5, pp. 950–959, Sep. 1992.

14. *COSMO-SkyMed SAR Products Handbook*, 2nd ed., Italian Space Agency, June 2009.

15. T. Fritz, S. Duque, B. Bräutigam, and J. L. B. Bello, "TanDEM-X experimental product description," Remote Sensing Technology Institute, Tech. Rep. TD-GS-PS-3028, Jan. 2012.

16. A. Ferretti, C. Prati, and F. Rocca, "Permanent scatterers in SAR interferometry," *IEEE Trans. Geosci. Remote Sensing*, vol. 39, no. 1, pp. 8–20, Jan 2001.

17. R. D. Chaney, A. S. Willsky, and L. M. Novak, "Coherent aspect-dependent SAR image formation," *Proc. SPIE*, vol. 2230, pp. 256–274, 1994.

18. G. S. Sammelmann, *Personal Computer Shallow Water Acoustic Tool-Set (PC SWAT) 9.0*, Naval Surface Warfare Center - Panama City Division, Oct. 2005.

19. J. A. Bucaro, B. H. Houston, M. Saniga, L. R. Dragonette, T. Yoder, S. Dey, L. Kraus, and L. Carin, "Broadband acoustic scattering measurements of underwater unexploded ordnance (UXO)," *J. Acoust. Soc. Am.*, vol. 123, no. 2, pp. 738–746, 2008.

20. K. L. Williams, S. G. Kargl, E. I. Thorsos, D. S. Burnett, J. L. Lopes, M. Zampolli, and P. L. Marston, "Acoustic scattering from a solid aluminum cylinder in contact with a sand sediment: Measurements, modeling, and interpretation," *J. Acoust. Soc. Am.*, vol. 127, no. 6, pp. 3356–3371, 2010.

21. J. Groen, "Adaptive motion compensation in sonar array processing," Ph.D. dissertation, Delft University of Technology, Jun. 2006.

22. J. W. Oeschger, "Estimating along-track displacement using redundant phase centers," in *Proceedings of the Institute of Acoustics*, vol. 28, no. 5, 2006.

23. D. A. Cook, "Synthetic aperture sonar motion estimation and compensation," Master's thesis, Georgia Institute of Technology, May 2007.